Hindawi
Geofluids
Volume 2022, Article ID 1117143, 16 pages
https://doi.org/10.1155/2022/1117143

WILEY | Hindawi

Research Article

Deformation Characteristics of Sandy Soil around a Plate Anchor under Lateral Loading

Miao Ren, Tong Jiang, Chen Liu, Junran Zhang, and Lijin Wang

Henan Province Key Laboratory of Geomechanics and Structural Engineering, North China University of Water Resources and Electric Power, Zhengzhou, Henan 450046, China

Correspondence should be addressed to Tong Jiang; 991641957@qq.com

Received 13 June 2022; Accepted 29 July 2022; Published 16 August 2022

Academic Editor: Daoyi Zhu

The lateral loading of a plate anchor is a complicated process that involves complex anchor-soil interactions. The deformation characteristics of the soil around an anchor have an important effect on its lateral bearing capacity. In this paper, the noncontact digital image correlation (DIC) technique is used to study the distribution and variation of the soil deformation field under a laterally loaded anchor in sandy soil. The results show that the sand density and embedment ratio significantly affect the distribution and influence range of the active and passive zones around the anchor. The active zone behind the rod gradually decreases with increasing sand density until ultimately disappearing, and the passive zone increases. The maximum influence height occurs in the passive zone behind the rod in dense sand, and the influence range of the passive zone in front of the rod expands with an increasing embedment ratio. Shear bands form during the lateral loading process, which are accompanied by dilatancy in the shear process. The motion path of the rotation center in loose and medium sand is initially rigid translational and then becomes rigid rotational, while the opposite trend occurs in compact dense sand. The results provide important guidance for the development of predictive models for anchor lateral loading and design.

1. Introduction

Plate anchors are widely used in transmission equipment foundations, TV towers, large suspension bridges, aircraft mooring platforms, and other fields owing to their short construction time, strong site applicability, reduced environmental damage, and good economic benefits. The extended development of energy exploitation in the deep sea in recent years has led to a gradual replacement of shallow sea gravity platforms with floating platforms. A plate anchor buried on the seabed provides the anchoring force for a floating platform to resist the impact of wind, waves, and sea currents, which are a wide concern in marine engineering [1].

Extensive research has been conducted to constrain the pullout bearing capacity of plate anchors using a variety of research methods, including theoretical studies [2–5], numerical simulations [6–13], and model texts [14–16], most of which are summarized in Das et al. [17] and Niroumand and Kasim [18]. The lateral bearing capacity and lateral tensile mechanism of laterally loaded plate anchors are jointly affected by the anchor and anchor rod, and the anchor-soil interactions are complicated. A calculation model of the lateral bearing capacity is therefore difficult to establish. There have been relatively few studies on the tensile mechanism of laterally loaded plate anchors in contrast to the extensive research that has been conducted on pile lateral loads [19–27]. Previous studies on the pull-out resistance of plate anchors and pile lateral loads mainly focused on the force or deformation of the anchor and pile, whereas research on the interaction characteristics of an anchor (pile) and surrounding soil and the deformation characteristics of the soil around the anchor (pile) remains poorly constrained. Digital image correlation (DIC) technology has been increasingly applied in geotechnical engineering model tests in recent years [28–34]. In particular, Liu et al. [35] and

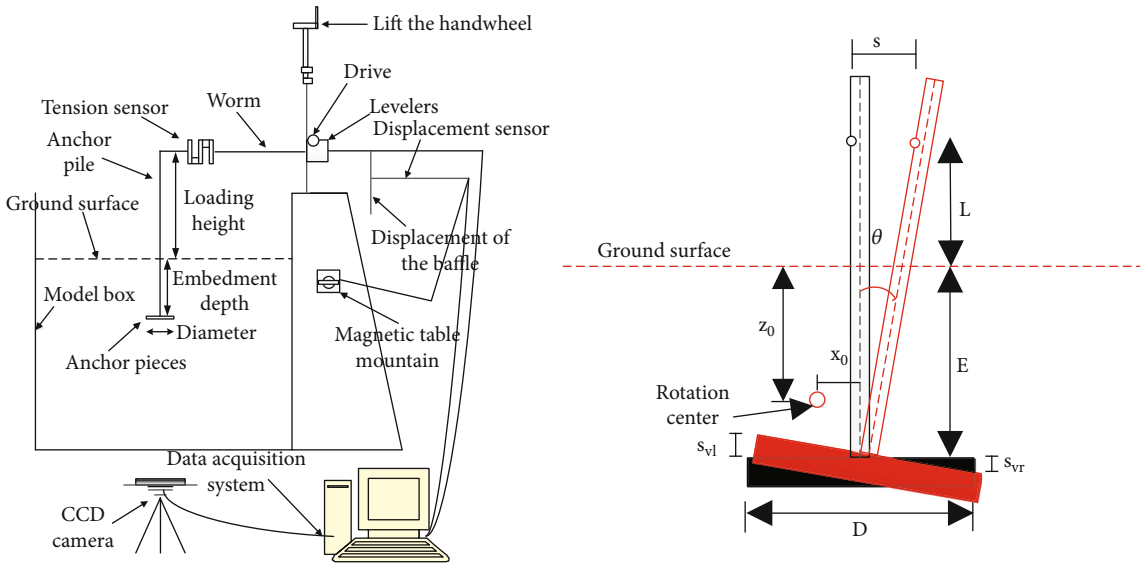

Figure 1: The experimental system.

Table 1: The definition of symbols.

Symbol	Definition
D (mm)	Diameter of plate anchor
E (mm)	Buried depth of plate anchor
S (mm)	The displacement of the anchor rod at the loading height
P (N)	Lateral load of the anchor rod at the loading height
L (mm)	The height of loading from the surface
x_0 (mm)	The offset of the rotation center relative to the centerline of the plate anchor foundation
z_0 (mm)	The depth of the rotation center below the ground surface
θ (°)	Rotation of plate anchor

Table 2: Parameters of the test program.

Number	D_r	φ (°)	E (mm)	(E/D)	L (mm)
1	$D_r = 27\%$	30.3	50–350	1–7	200
2	$D_r = 55\%$	33.1	50–350	1–7	200
3	$D_r = 75\%$	37.1	50–350	1–7	200

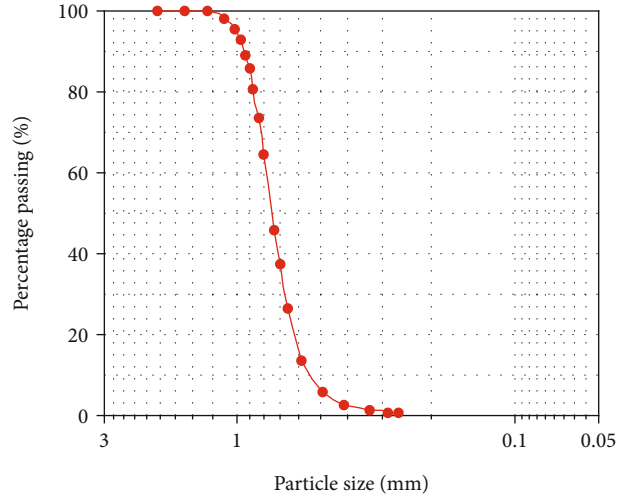

Figure 2: Particle grading curve of the soil sample.

Zhang et al. [36] used DIC technology to conduct an experimental study on the soil deformation mechanism around an anchor during the process of removing a single anchor and group of anchors in sand.

DIC technology is used in this study to design a set of lateral loading devices and a data image acquisition system for plate anchors. The deformation field of the soil around a plate anchor is measured and analyzed under different sand density and embedment ratio conditions, which is helpful to monitor the development and change of the deformation field of the soil around a plate anchor and the interaction mechanism between the anchor and soil. Moreover, according to the movement characteristics of the soil around the plate anchor, the deformation field of the soil around the plate anchor is divided and the influence range of the displacement field around the anchor is quantitatively analyzed, which can improve the reference for the foundation treatment. The inner law of the mechanical phenomenon is deeply analyzed from the

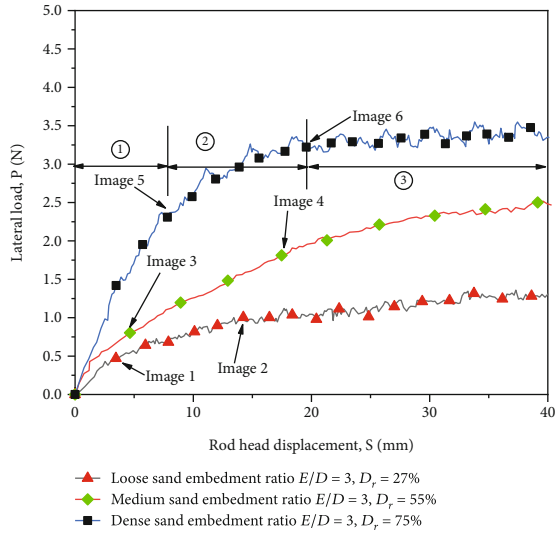

(a) Load-displacement curves with variable D_r values

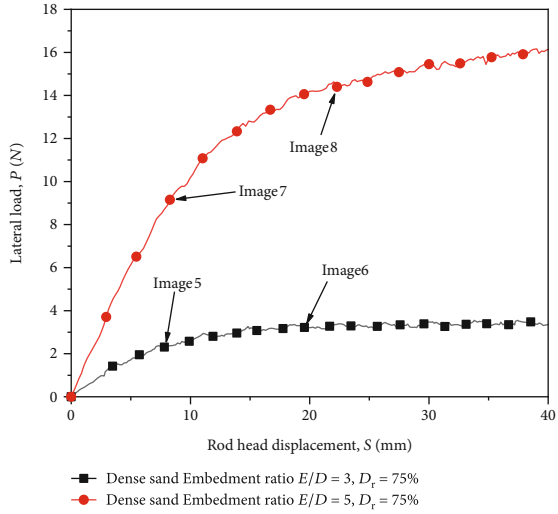

(b) Load-displacement curves with variable E/D values

Figure 3: Relationship between lateral load and rod head displacement for different influencing factors.

Table 3: Information for images corresponding to points along the lateral load and displacement curve.

Number	Relative density and embedment ratio	Image number	Rod head displacement S (mm)	Lateral load P (N)
1	$D_r = 27\%$, $E/D = 3$	1	2.33	0.36
		2	14.23	1.01
2	$D_r = 55\%$, $E/D = 3$	3	4.64	0.80
		4	17.5	1.81
3	$D_r = 75\%$, $E/D = 3$	5	7.33	2.37
		6	18.36	3.35
4	$D_r = 75\%$, $E/D = 5$	7	9.26	9.78
		8	22.02	14.68

perspective of the deformation field, and the deformation and failure mechanism of the soil around the anchor plate during the lateral loading process is revealed. The test results can provide a reference for the establishment and design of the anchor plate lateral bearing capacity prediction model for practical engineering.

2. Materials and Methods

2.1. Experimental Setup. The developed experimental system (Figure 1) mainly consists of a loading device, a DH3821 data acquisition instrument, and an image analysis system, the latter of which includes a high-speed CCD

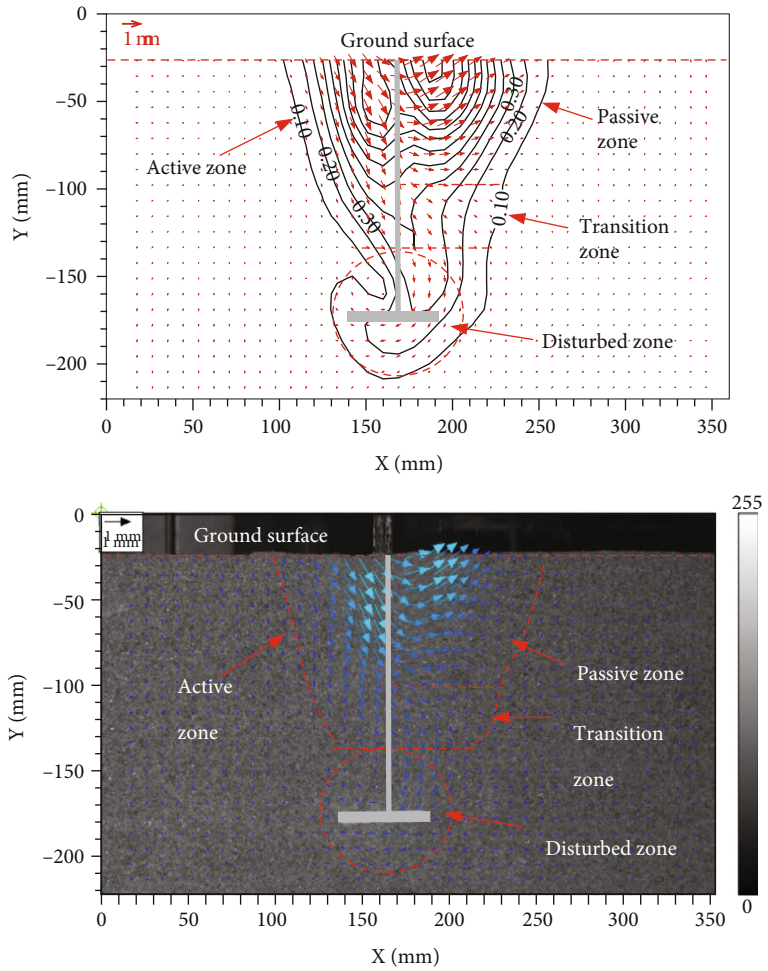

Figure 4: Displacement field at the ultimate load under conditions of $D_r = 27\%$ and $E/D = 3$.

camera and StrainMaster of DaVis 8.0 software. The loading device is mounted on a height-adjustable lifter, which provides a hole through which the worm can pass and move left and right using the drive of the worm gear. A DH3821 machine is used to apply a lateral force and measure the displacement of the plate anchor. The high-speed CCD camera is used with a Sony scientific research chip with a resolution of 2489 × 2091 pixels. DaVis 8.0 is an embedded DIC software used to analyze the relative movement between any two images. The image acquisition frequency of the force and displacement is 2 Hz, which achieves synchronization.

A model tank with dimensions of 800 × 600 × 700 mm (length × width × height) was developed to install the screw anchor pile. The plate anchor consists of an anchor rod and anchor. The rod body is made of a steel shaft with a diameter of 7 mm. The anchor is half-circular with a diameter of 50 mm and thickness of 5 mm. The relevant symbols are defined in Table 1.

2.2. Test Program. The test program is presented in Table 2 and mainly considers the following test parameters: sand density (loose, medium, and dense), embedment ratio (E/D of 1–7, where E is the embedment depth and D is the anchor diameter), and load height ($L = 200$ where L

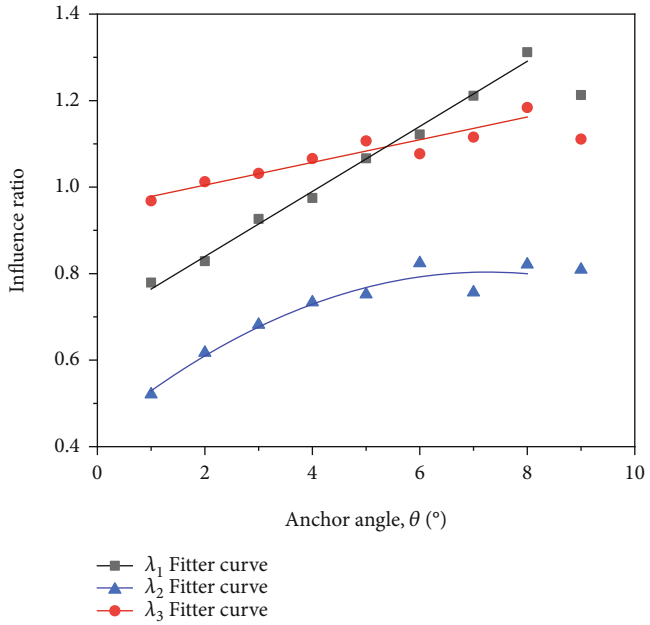

Figure 5: Influence ratio of the soil displacement as a function of anchor angle for $D_r = 27\%$ and $E/D = 3$.

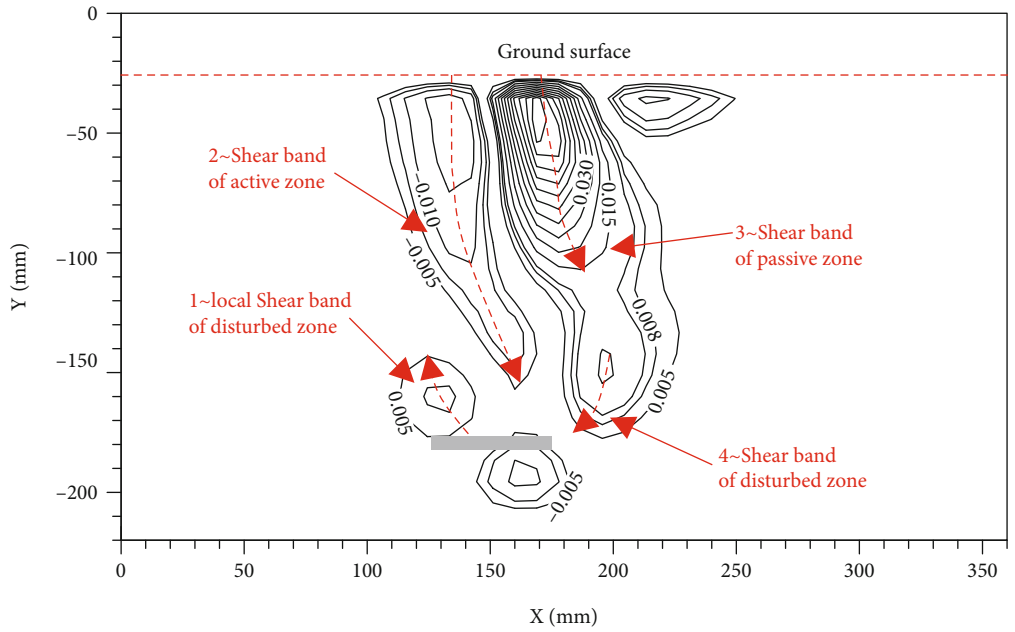

Figure 6: Shear strain field at the ultimate load for $D_r = 27\%$and $E/D = 3$.

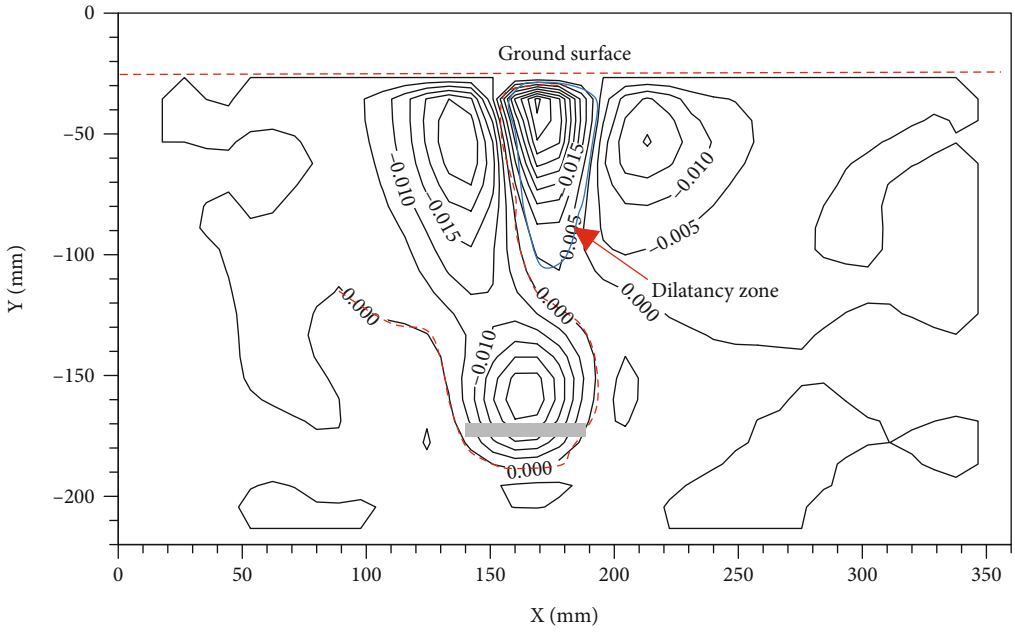

Figure 7: Volume strain field at the ultimate load for $D_r = 27\%$and $E/D = 3$.

is the distance from the lateral loading application location to the ground surface).

2.3. Starting Material. The sand saturation is dry sand, and sand of different densities was used to study the influence of density on the sand deformation and failure mechanism around a screw plate anchor. These include loose sand (average dry density $\rho_d = 1.47\ g/cm^3$, corresponding to a relative density of $D_r = 27\%$), medium sand ($\rho_d = 1.53\ g/cm^3$, $D_r = 55\%$), and dense sand ($\rho_d = 1.61\ g/cm^3$, $D_r = 75\%$). The angles of friction corresponding to the loose, medium, and dense sand conditions were 30.3°, 33.1°, and 37.1°, respectively. The physical properties were obtained by referring to GB/T 50123-2019 [37], and the sand particle size distribution curve is presented in Figure 2.

2.4. Experimental Procedure. The position and height of the camera were first adjusted to capture the area of interest. Because images are sensitive to changes in ambient light, the focus and light intensity were adjusted to achieve good image quality. The sensors and power supply were then checked, the data acquisition software was started,

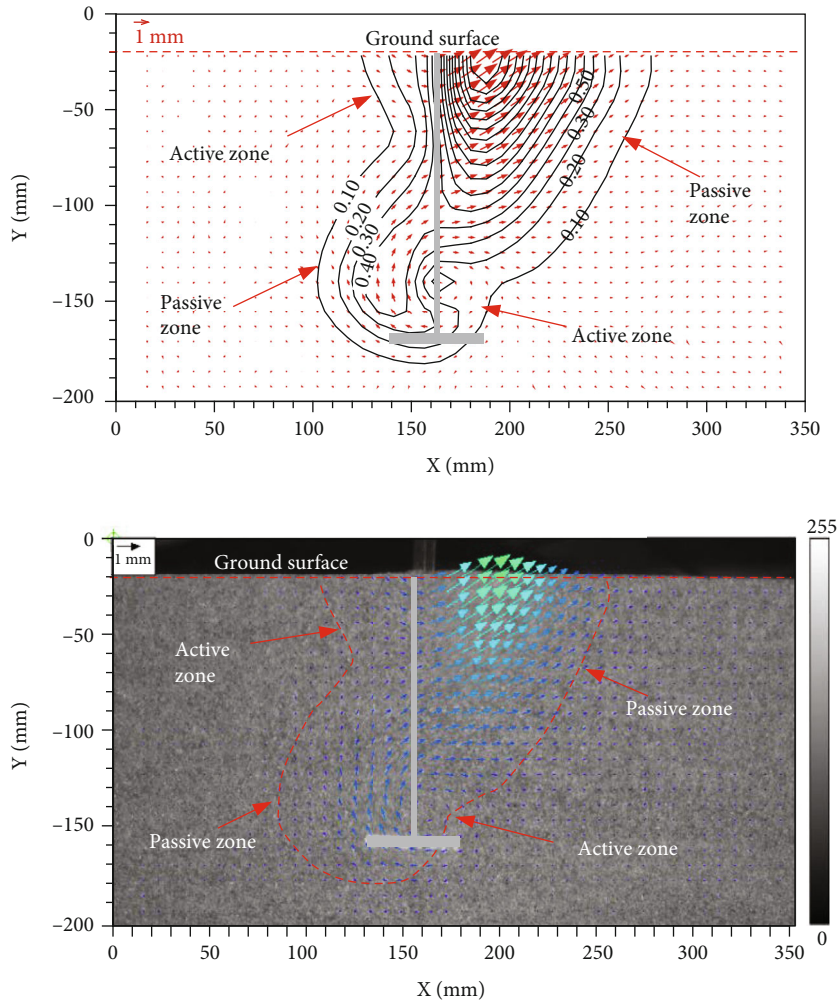

Figure 8: Displacement field at the ultimate load for $D_r = 55\%$ and $E/D = 3$.

the acquisition parameters were set, and the collection system initiated the loading device. During loading, the plate anchor speed was controlled at 0.01 mm/s to minimize the impact of the loading speed on the load and allow sufficient images to be collected prior to reaching the ultimate load. At the end of the test, the data were saved and the lateral load and displacement curves were plotted.

3. Results and Analyses

3.1. Lateral Load versus Displacement Response. The relationship between the lateral load and rod head displacement for different D_r and E/D values was compared and analyzed under the same test conditions to study their effects on the lateral tensile resistance characteristics of the plate anchors. Figure 3(a) shows the relationship between the lateral load and rod head displacement in loose, medium, and dense sand for $E/D = 3$. This relationship curve can be divided into three stages during the lateral loading process of the plate anchor: an elastic stage, an elastoplastic stage, and a strong reduction stage. (a) In the elastic stage, the lateral load

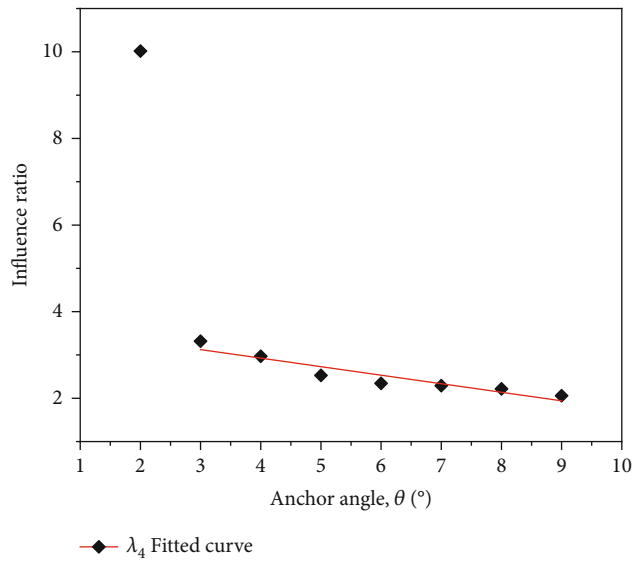

Figure 9: Influence ratio of the soil displacement as a function of anchor angle for $D_r = 55\%$ and $E/D = 3$.

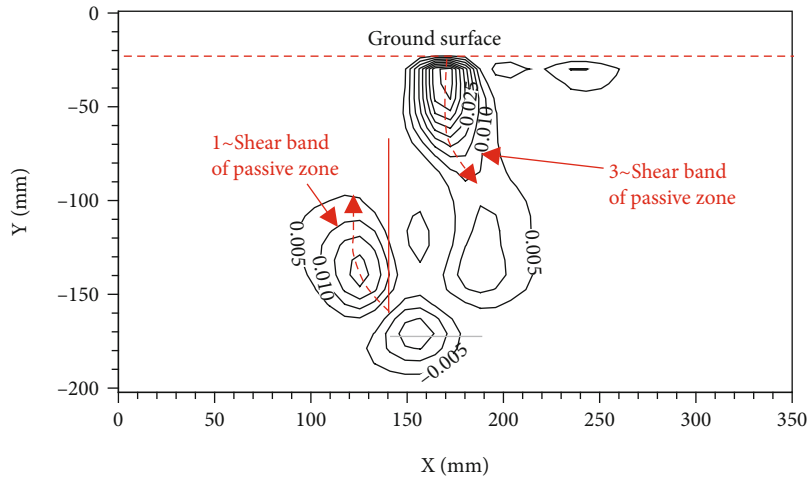

Figure 10: Shear strain field at the ultimate load for $D_r = 55\%$ and $E/D = 3$.

increases linearly with displacement, and the slope of the linear segment increases with increasing sand density. (b) In the elastoplastic stage, the rate at which the load increases with increasing displacement slows relative to that in the previous stage. The ultimate lateral load is considered to be the point where the load versus rod head displacement curve becomes linear [21]. The ultimate lateral loads of the loose, medium, and dense sand curves are 1.01, 1.75, and 3.35 N, respectively, which shows that increasing sand density has a significant effect on the lateral bearing capacity. (c) In the strong reduction stage, the displacement increases dramatically while the load changes slightly, which is consistent with the typical curve of dense sand characteristics. Figure 3(b) shows the relationship between the lateral load and rod head displacement for different E/D values in dense sand. The two curves show similar characteristics: the linear slope of the curve during the first stage for $E/D = 5$ ratio is approximately 4.4 times steeper than that for $E/D = 3$, which indicates that E/D has also a significant impact on the lateral bearing capacity.

3.2. Soil Deformation Field in Loose Sand. The lateral loading tests under different sand density and embedment ratio conditions were selected to analyze the soil deformation field around a plate anchor during the lateral loading process. Images 1–8 in Figure 3 correspond to the ultimate lateral load and rod head displacement under four different working conditions. The ultimate lateral load and displacement at the corresponding points of each image are listed in Table 3.

The displacement field of the first group of images under the ultimate load was obtained after the DIC calculation, as shown in Figure 4. The arrow in the upper-left corner shows the displacement reference value and represents the displacement magnitude and direction. The front of the rod refers to the side along the loading direction, and the back of the rod refers to the side away from the loading direction. The displacement field indicates that the soil around the plate anchor is displaced, and the contours of the front and back of the anchor rod approximate a parabola with an upward opening. If the anchor rod is regarded as the back of the gravity retaining wall and the interaction between the rod and soil is regarded as the retaining wall rotating around the wall toe, active and passive zones are observed to form on the front and back sides of the rod, respectively. The soil particles in the active zone behind the rod flow downward to the right, and the surface and underground influence range from 1.6 D to 2.2 D. The movement direction of the soil particles in the front of the rod goes through the upper-right side of the near surface, the lower-right side of the middle zone, and the lower-left side of the upper part of the anchor. The three zones are named as the passive zone, transition zone, and active zone, respectively, and are bounded by the change of the soil particle movement direction. The influence ranges of the surface and underground in the passive zone in front of the rod are 1.6 D and 1.4 D, respectively. An approximate circular displacement field forms around the anchor, with the center of the circle located at the center of the anchor and an influence diameter of approximately 1.2 D. The soil in this area is jointly affected by the lateral loading process of the anchor and anchor rod. The anchor-soil interaction is complicated; thus, this area is referred to as the disturbance zone.

The influence range of the displacement field is treated as a dimensionless quantity to study the deformation characteristics of the soil displacement field around the plate anchor during the lateral loading process. Statistical analysis is performed to determine the surface influence width ratio before and after the rod (λ_1), influence depth ratio (λ_2), influence range ratio (λ_3), and the change of anchor angle (θ) using a contour range of 0.10 as the boundary. The relationships between the correlation ratio and anchor angle in Figure 5 show that λ_1 and λ_3 increase linearly with θ for $\theta < 8^\circ$ and that λ_2 and θ follow a parabolic relation. The ratio of the surface width is notably larger than that of depth, which indicates that the influence range of the active and passive areas is strongly affected by the surface width and the ratio decreases for $\theta > 8^\circ$.

Figure 6 shows the shear strain field at the ultimate load in loose sand. Approximately 1–4 shear bands are noted from left to right, and the maximum shear strain points

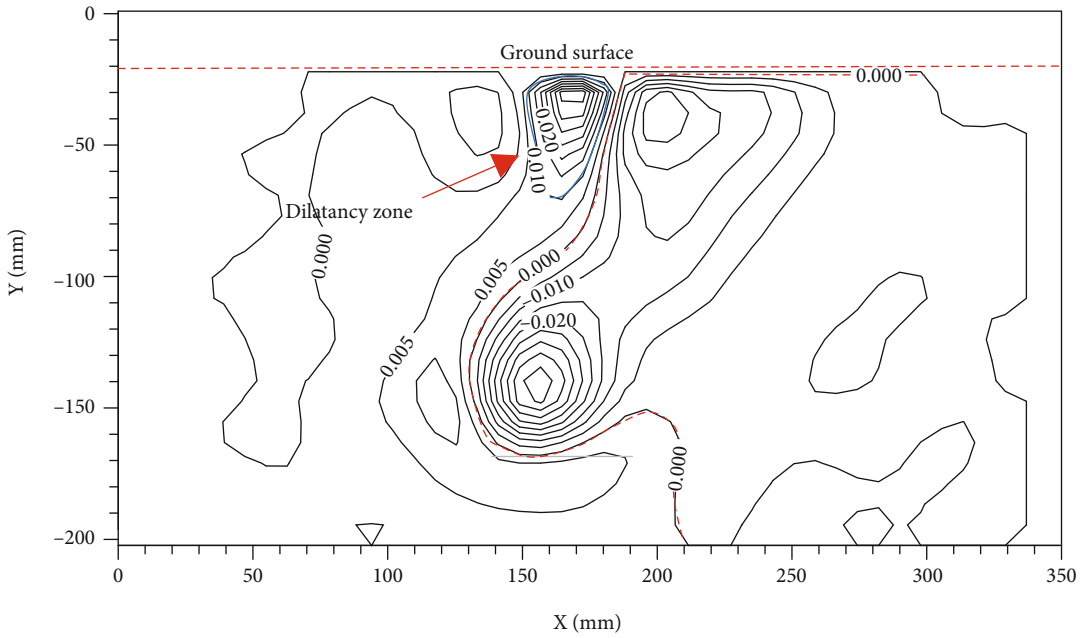

Figure 11: Volume strain field at the ultimate load for $D_r = 55\%$ and $E/D = 3$.

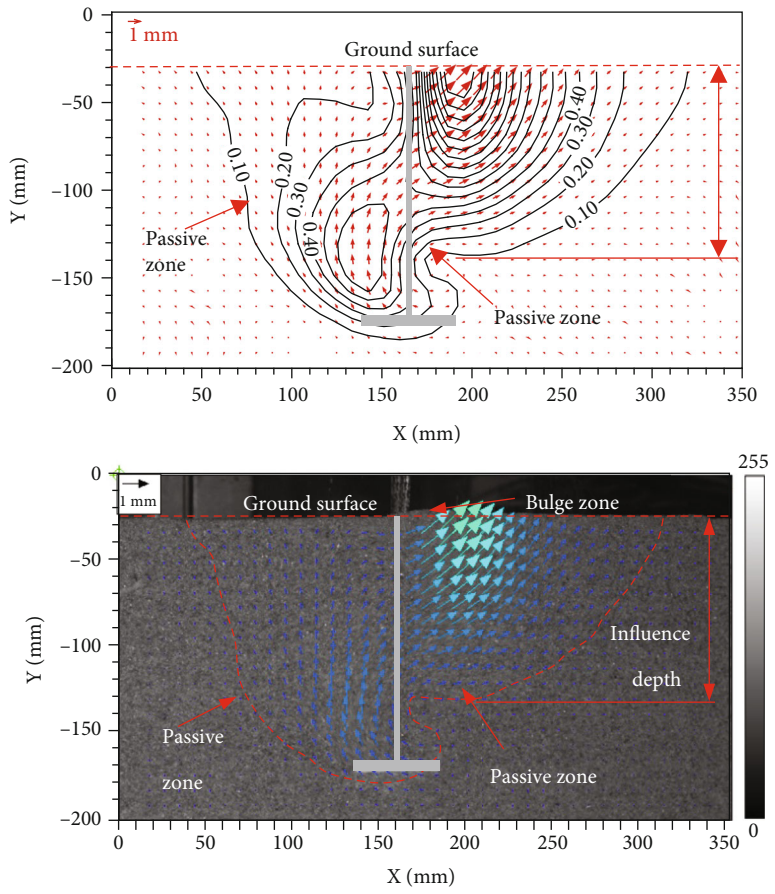

Figure 12: Displacement field at the ultimate load for $D_r = 75\%$ and $E/D = 3$.

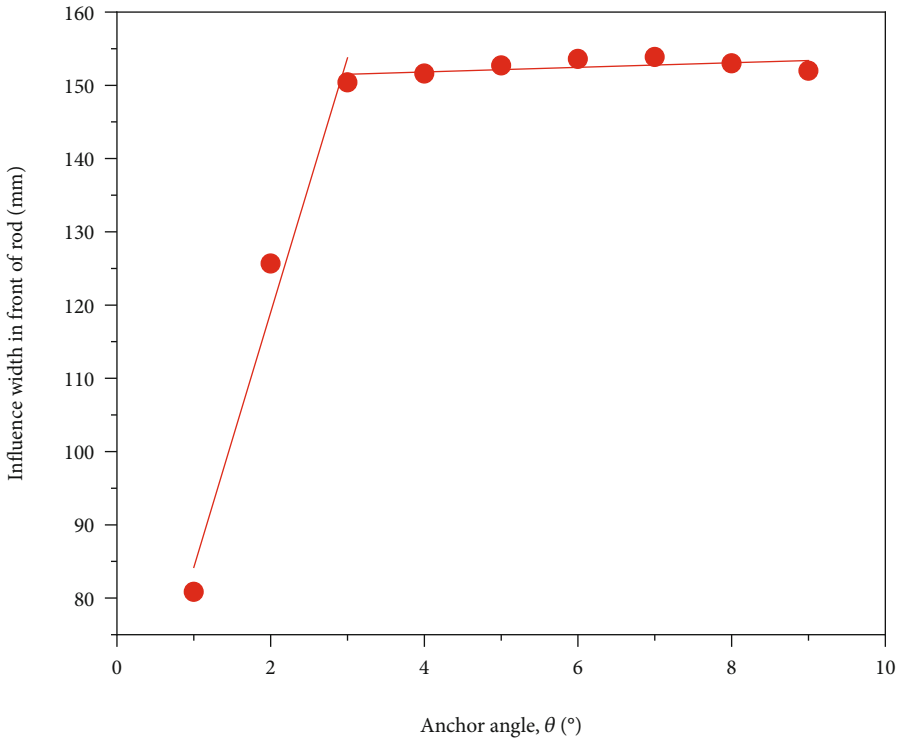

(a) Influence width in front of the rod as a function of the anchor angle

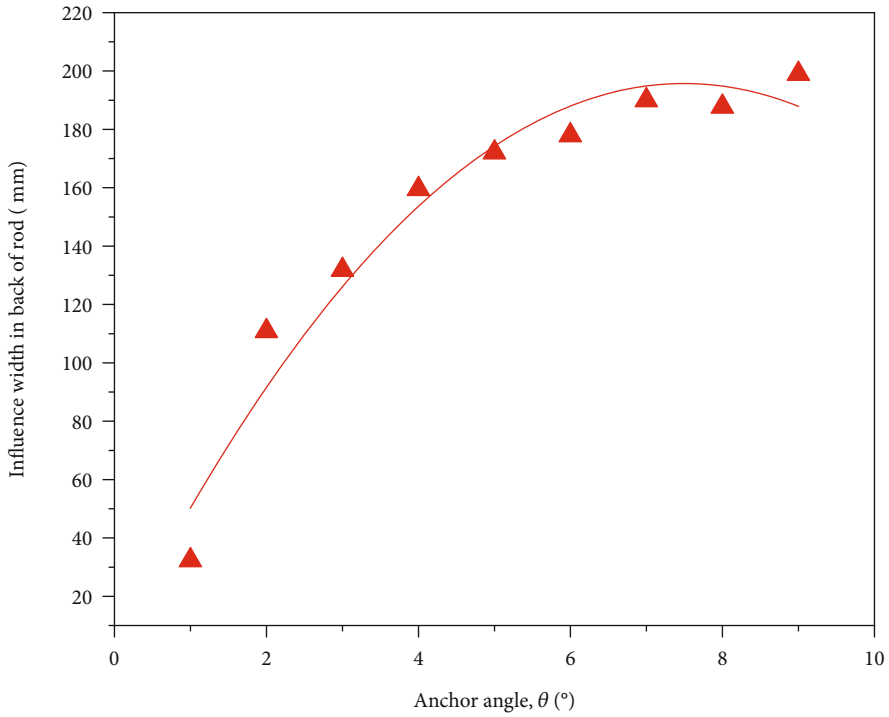

(b) Influence width in back of the rod as a function of the anchor angle

Figure 13: Continued.

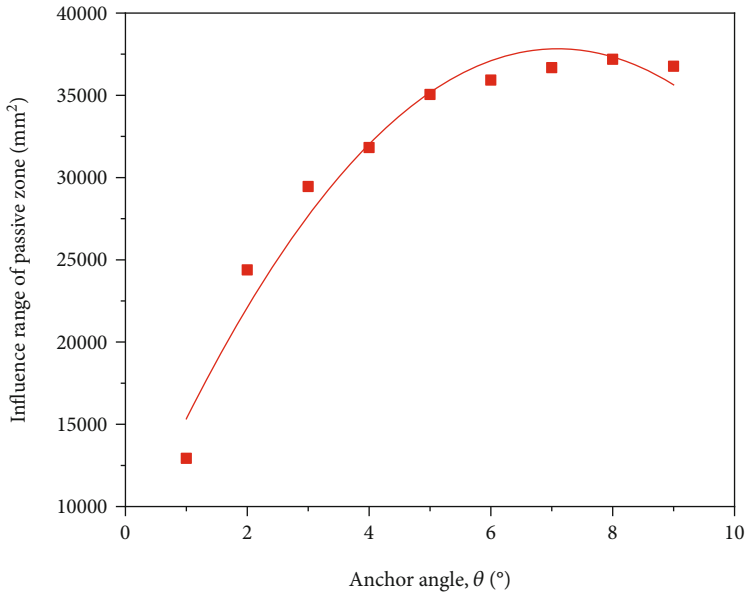

(c) Influence range of the passive zone as a function of the anchor angle

Figure 13: Influence range as a function of the anchor angle.

in the shear strain isoline map connect as a shear surface of lateral tensile failure of the plate anchor. Local shear band #1 forms on the left edge of the anchor, extends to the upper part of the anchor by approximately 0.6 D, and is located in the disturbance zone on the upper left of the anchor. Shear band #2 extends from the ground surface to the lower right, which the same direction as the soil particle movement in the active zone behind the rod. Shear band #3 is located in the passive zone behind the rod and affects the depth over a range of 1.6 D. Shear bands #2 and #3 gradually shrink with increasing depth mainly owing to increasing soil stress, which is also associated with a reduction of the dilatancy angle. Shear band #4 extends from 0.6 D to the lower left of the anchor and forms a local shear band located in the disturbance area on the upper-right side of the anchor.

Figure 7 shows the volumetric strain field at the ultimate load in loose sand. The red dotted line represents the division between positive volumetric strain values, which indicate volume expansion, and negative volumetric strain values, which indicate volume compression. The range of the solid blue line indicates the dilatancy zone, which is located in the passive zone behind the rod and is consistent with the distribution of shear band #3. The shear shrinkage zone is mainly located in the active zone behind the rod and disturbance zone above the anchor. The loose soil in the active zone in back of the rod becomes dense and forms a shear shrinkage zone. The pressure difference of the soil above the anchor occurs during the rotation of the anchor rod, which leads to soil compression and shear shrinkage.

3.3. Soil Deformation Field in Medium Sand. Figure 8 shows the displacement field at the ultimate load in medium sand. The transition zone in front of the rod is less apparent than that in the loose sand scenario, and the influence depth of the passive zone increases to 2D below the ground surface. This indicates a weakened influence of the anchor rotation and enhanced passive extrusion effect of the rod. The influence range of the active zone behind the rod strongly increases from 0.8 D in loose sand to 2.2 D in medium sand. The influence of the left anchor rotation on the soil movement increases, as well as the influence of the passive zone. The disturbed area around the anchor contracts and the passive area affects the expansion.

Figure 9 shows the relationship between the surface influence width ratio λ_4 before and after the rod and the anchor angle. The active zone behind the rod is not apparent for $\theta < 3^\circ$ and the ratio is large, whereas the ratio is small for $3^\circ < \theta < 9^\circ$ and decreases linearly with θ.

Figure 10 shows the shear strain field at the ultimate load in medium sand. Compared with the loose sand scenario, the influence height of shear band #1 on the upper-left side of anchor increases and extends to the upper part of the anchor over 1.4 D, whereas shear bands #2 and #4 disappear and shear band #3 in front of the rod extends below the ground surface for 1.4 D and decreases. The volumetric strain field in Figure 11 shows that the dilatancy zone shrinks with increasing relative density and the shrinkage zone behind the rod is not apparent.

3.4. Soil Deformation Field in Dense Sand. Figure 12 shows the displacement field at the ultimate load in dense sand. As the relative density increases, the active zone behind the rod disappears and the soil particles are mainly affected by the rotation of the anchor and move upward to the left. This forms a passive zone, and the displacement contour is approximately "ear" shaped. The influence

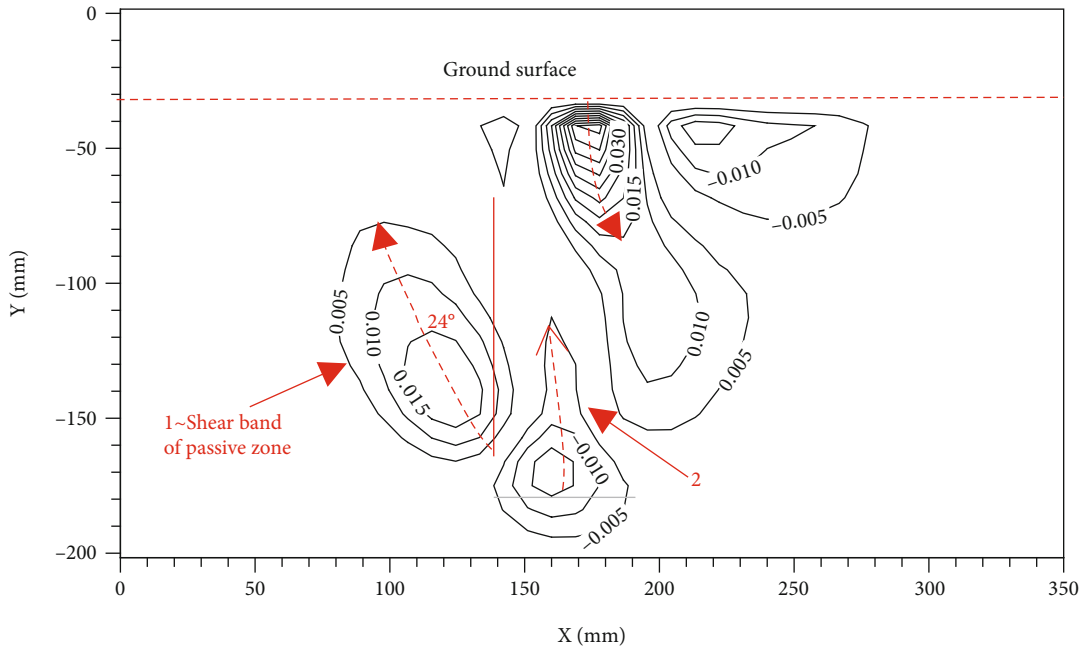

Figure 14: Shear strain field at the ultimate load for $D_r = 75\%$ and $E/D = 3$.

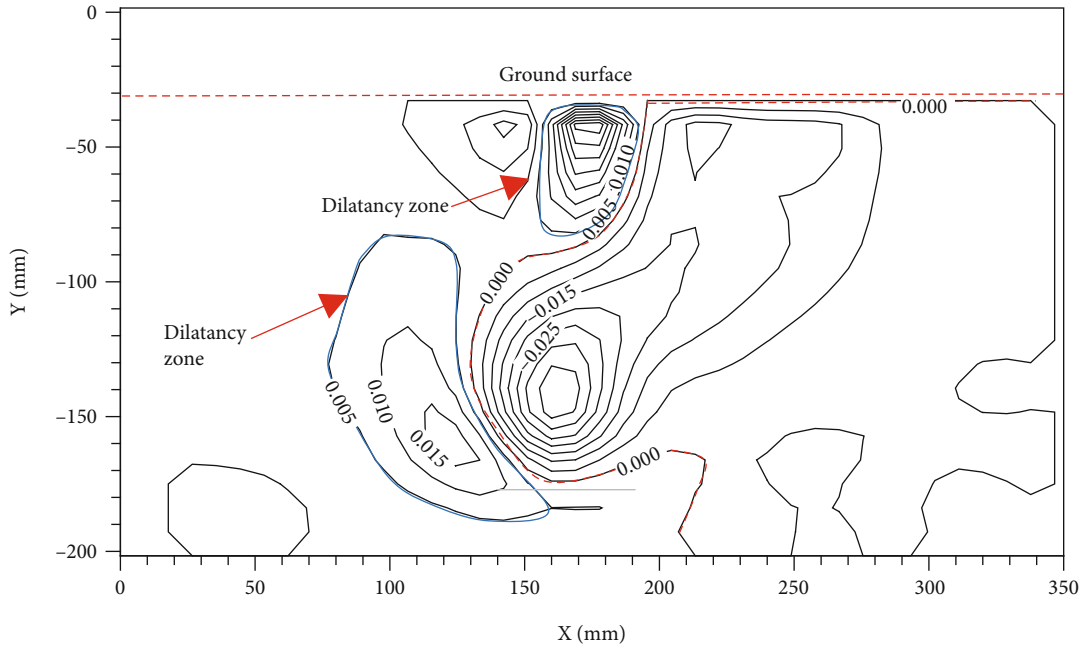

Figure 15: Volume strain field at the ultimate load for $D_r = 75\%$ and $E/D = 3$.

depth of the passive zone in front of the rod continues to increase to approximately 2.2 D. The influence width of the surface passive zone notably expands obviously with increasing sand density. The passive area is mainly around the anchor.

The soil around the plate anchor in dense sand is dominated by the passive zone. The influence width of the ground surface and influence range of the passive zone with changing rod inclination are statistically analyzed. Figure 13 shows the relationship between the influence range of the passive zone and rod inclination. Figure 13(a) shows that the influence width of the ground surface in front of the rod increases linearly for rod inclination values less than 3° and remains essentially unchanged between 3° and 9° to a maximum influence height of 3 D. Figures 13(b) and 13(c) show that the influence width of the ground surface behind the rod and the sum of the passive zone before and after the rod follow a parabolic relationship for rod inclination values less than 9°. Because the influence depths of the passive zone in front of and behind the rod are essentially maintained at 2.2 D and 3 D,

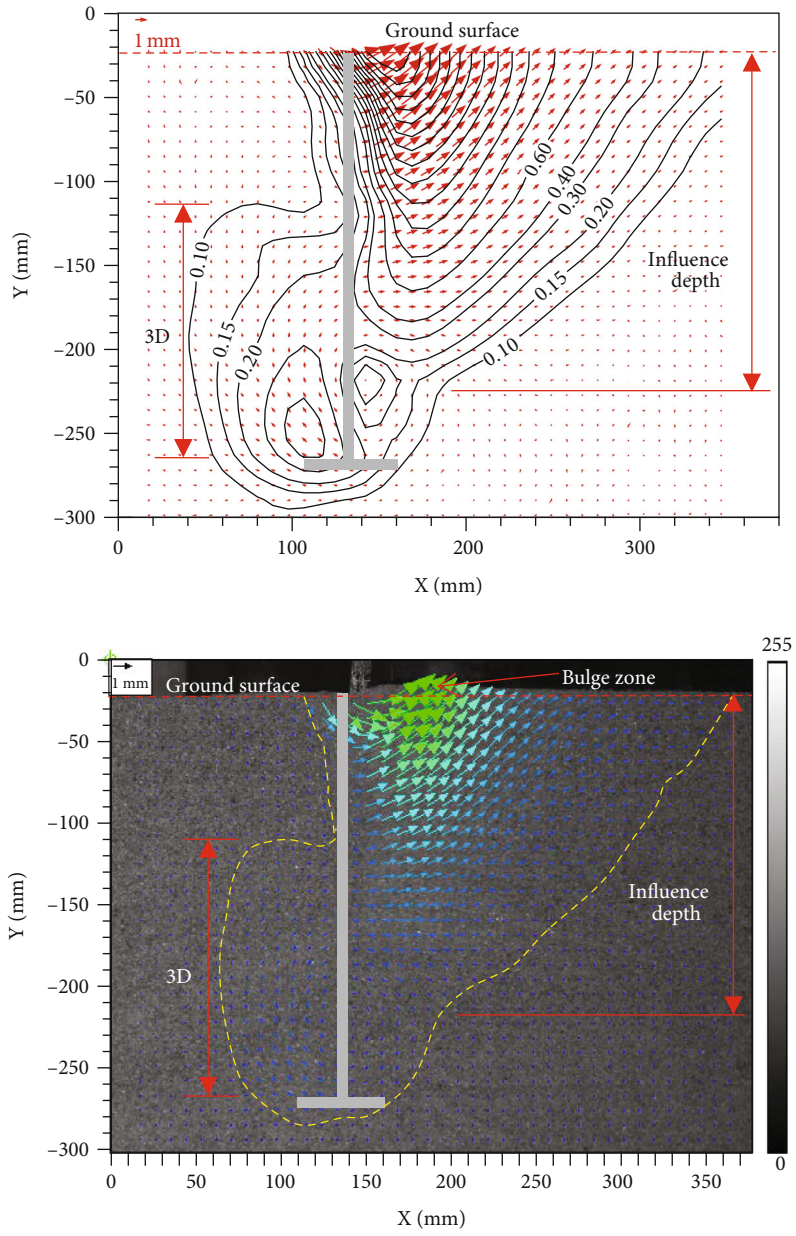

Figure 16: Displacement field at the ultimate load for $D_r = 75\%$ and $E/D = 5$.

respectively, the surface influence width of the latter plays a major role in the influence range of the passive zone.

Figure 14 shows the shear strain field at the ultimate load in dense sand. Shear band #1 extends from the left edge of the anchor to the upper left with an influence height of approximately 2 D, which is much larger than that in loose sand. The angle between the shear plane and vertical direction is 24°. Shear band #2 extends from the surface of the anchor to the upper left, which is contrary to the ground surface extension to the lower right in loose sand. The increased extension range of shear band #1 and altered extension direction of shear band #2 are the main reasons for the increased ultimate load. The surface depth of shear band #3 continues to shrink downward to approximately 1.2 D mainly owing to the increased sand density, which increases the soil stress level.

Figure 15 shows the volumetric strain field at the ultimate load in dense sand. Compared with the loose and medium sand scenarios, a notable dilatancy zone forms on the left edge of the anchor, which is consistent with shear band #1.

3.5. Effect of the Embedment Ratio on the Deformation Field in Dense Sand. Figures 16–18 show the deformation field at the ultimate load in dense sand with $E/D = 5$. The shape of the displacement field in Figure 16 remains essentially unchanged from that for $E/D = 3$. The influence depth of the displacement field behind the rod is approximately 3D, which is the same as for $E/D = 3$, indicating that the

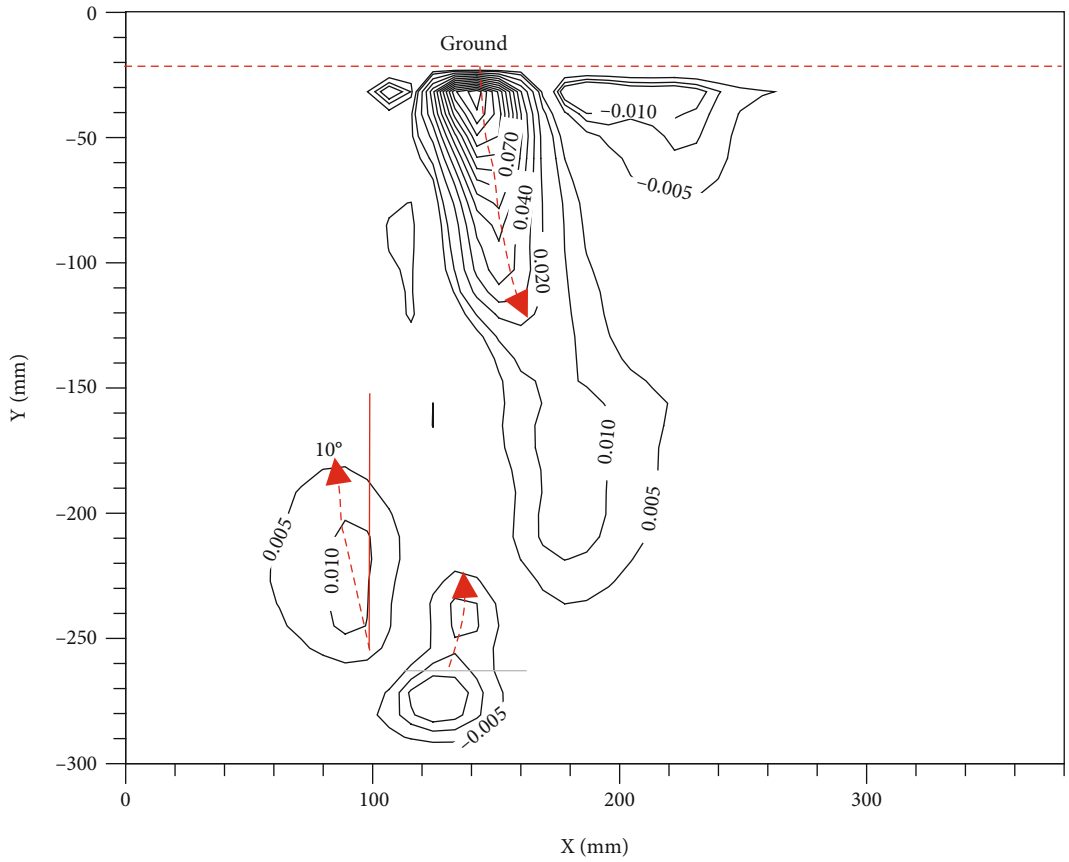

Figure 17: Shear strain field at the ultimate load for $D_r = 75\%$ and $E/D = 5$.

increased E/D has little effect on the extension height of the passive zone behind the rod. The affected depth of the rod front is 4 D, which is 1.8 times larger than that for $E/D = 3$, and the range of the uplifted area is enlarged. The shear strain field in Figure 17 shows that shear band #1 inclines inward and the angle between the shear failure surface and vertical direction is 10°, which is smaller than that for $E/D = 3$. The upward extension range of shear band #2 is small mainly because the lateral soil stress increases with depth. The volumetric strain field in Figure 18 shows that the dilatancy zone above the anchor becomes long and narrow with an affected depth of approximately 2.6 D, which is significantly larger than that for $E/D = 3$. Furthermore, the dilatancy at the left edge of the anchor is not apparent.

3.6. Evolution of the Rotation Center Position under Lateral Loading. The position of the plate anchor's rotation center under lateral loading is an important input condition to calculate the foundation bearing capacity using traditional analytical methods. The rotational center position of the foundation is therefore calculated in reverse according to the displacement meter arranged at the lateral pulling position of the anchor rod and the plate anchor coordinates on the acquired images. This provides a reference for future studies to analyze the anchor plate foundation. The schematic diagram of the rotation center of the anchor plate can be seen in Figure 1. The lateral rotation center and depth below the ground surface can be calculated according to the following:

$$x_0 = \frac{D}{2} \times \frac{S_{vl} - S_{vr}}{S_{vl} + S_{vr}},$$
$$z_0 = \frac{D \times S}{S_{vl} + S_{vr}} - L. \quad (1)$$

Figure 19 shows the movement path of the plate anchor foundation's rotation center under lateral loading. A Cartesian coordinate system is defined whose center corresponds to the center of the plate anchor foundation at the ground surface elevation. For the plate anchor foundation, the lateral coordinates of the rotation center are treated as the dimensionless plate anchor diameter (D), whereas the vertical coordinates of the rotation center are normalized by the plate anchor embedment depth (E). Figure 19 illustrates that sand density has a strong effect on the movement path of the rotation center for a plate anchor in sandy foundations under applied lateral force. The original basis of the rotation center is located in the vertical center line to the left of 0.44 D to 0.72 E. The rotation center of plate anchor foundation moves to the vertical center line with increasing lateral load. This shows that the foundation movement mode at this time is mainly rigid translational. As the load continues to increase for an anchor rod rotation angle of 6°, the rotation center is stable near the center line, which is located around 0.8 E

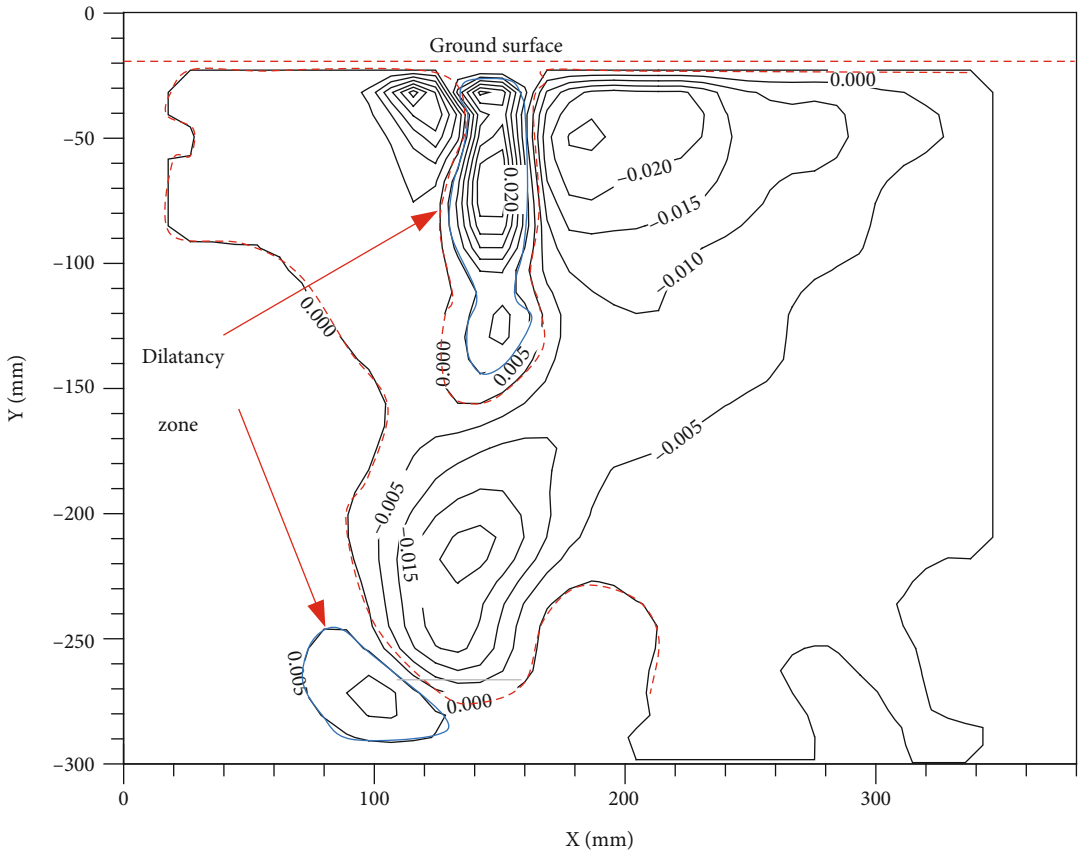

Figure 18: Volume strain field at the ultimate load for $D_r = 75\%$ and $E/D = 5$.

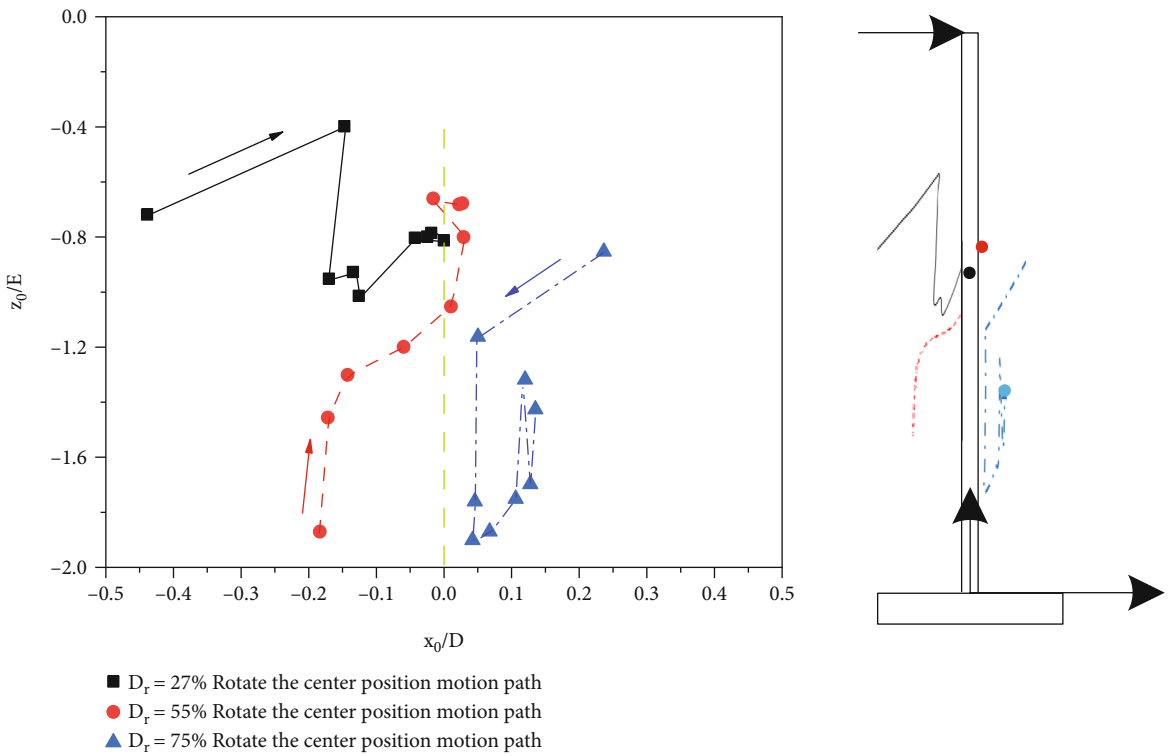

Figure 19: Rotation path of the center position's motion.

below the ground surface, indicating that the movement mode of the plate anchor foundation at this time is mainly rigid rotation. For the plate anchor foundation in medium sand, the motion form of the rotation center is the same as that of loose sand. The rotation center first moves, then rotates, and finally stabilizes at 0.02 D to the left of the centerline and around 0.68 E below the ground surface. The movement path of the plate anchor foundation's rotation center in dense sand is notably different from those in loose and medium sand. When the initial lateral force is applied, the rotation center of the plate anchor foundation is located at 0.24 D to the right of the vertical center line and 0.85 E below the ground surface. The rotation center of plate anchor foundation moves to the vertical center line with increasing lateral load when the rod inclination is 2°. The rotation center is stable near the center line (left 0.05 D), and the rotation center simultaneously moves downward, which indicates that the motion mode at this time is mainly rigid rotation. As the lateral load continues to increase, the rotation center moves away from the center line, indicating that the foundation movement mode at this time is dominated by rigid translation.

4. Discussion and Conclusion

This article presents an experimental investigation of the interaction between plate anchors and soil using an optical setup. The test setup includes a loading frame, camera, and computer equipped with DIC software. A series of scale model tests were performed to study the deformation characteristic of sandy soil around plate anchors under different sand density and embedment ratio conditions. The conclusions from this research are summarized as follows:

(i) Increased sand density and embedment ratio lead to increased slopes of the lateral load versus rod head displacement curves in the elastic stage at the ultimate load

(ii) The active zone behind the rod decreases gradually with increasing sand density until disappearing, and the influence range of the passive zone around the anchor gradually increases. The maximum influence height of the passive zone behind the rod in dense sand is 3D, and the passive zone in front of the rod expands with increasing embedment ratio

(iii) The influence range of the active and passive zones on both sides of the rod and the rod inclination (< 9°) are sensitive to sand density, which provides a reference for improving the range of foundation treatment in practical engineering

(iv) The extension range of the shear band on the left edge of the anchor increases with increasing sand density, and the ground surface extension shear band on the lower right side of the active zone gradually shrinks until disappearing, forming a shear band on the upper left side of the anchor. During the shear process, the shear band in the passive zone is accompanied by shear dilatancy

(v) In loose and medium sand, the motion path of the rotation center is first rigid translational and then rigid rotational, whereas the opposite is observed in compact dense sand

Data Availability

No data were used to support this study.

Conflicts of Interest

The authors declare that they have no conflicts of interest.

Acknowledgments

This study is financially supported by the National Natural Science Foundation of China (Grant no. 41602295), the Foundation for University Key Teacher by the Ministry of Education of Henan Province (Grant no. 2020GGJS-094), the Key Scientific Research Projects of Colleges and Universities in Henan Province (Grant no. 21A410002), and the Doctoral Student Innovation Foundation of NCWU.

References

[1] K. Ilamparuthi, E. A. Dickin, and K. Muthukrisnaiah, "Experimental investigation of the uplift behaviour of circular plate anchors embedded in sand," *Canadian Geotechnical Journal*, vol. 39, no. 3, pp. 648–664, 2002.

[2] Z. A. Ardebili, M. A. Gabr, and M. S. Rahman, "Uplift capacity of plate anchors in saturated clats: analyses with different constitutive models," *International Journal of Geomechanics*, vol. 16, no. 2, article 04015053, 2016.

[3] A. S. Al-Suhaily, A. S. Abood, and M. Y. Fattah, "Bearing capacity of uplift piles with end gates," in *Proceedings of China-Europe Conference on Geotechnical Engineering, SSGG*, pp. 893–897, Nature Switzerland AG, 2018.

[4] J. D. Geddes and E. J. Murray, "Plate anchor groups pulled vertically in sand," *Journal of Geotechnical Engineering*, vol. 122, no. 7, pp. 509–516, 1996.

[5] R. Ganesh and J. P. Sahoo, "Seismic stability of obliquely loaded circular plate anchors," *Ocean Engineering*, vol. 217, article 107856, 2020.

[6] N. Al Hakeem and C. Aubeny, "Numerical modeling of keying of vertically installed plate anchor in sand," *Ocean Engineering*, vol. 223, no. 9, article 108674, 2021.

[7] X. Cheng, Y. Li, P. Wang, Z. Liu, and Y. Zhou, "Model tests and finite element analysis for vertically loaded anchors subjected to cyclic loads in soft clays," *Computers and Geotechnics*, vol. 119, article 103317, 2019.

[8] J. Kumar and N. Kouzer, "Vertical uplift capacity of a group of shallow horizontal anchors in sand," *Geotechnique*, vol. 58, no. 10, pp. 821–823, 2008.

[9] K. M. Kouzer and J. Kumar, "Vertical uplift capacity of equally spaced horizontal strip anchors in sand," *International Journal of Geomechanics*, vol. 9, no. 5, pp. 230–236, 2009.

[10] J. Liu, M. Tan, and Y. Hu, "New analytical formulas to estimate the pullout capacity factor for rectangular plate anchors in NC clay," *Applied Ocean Research*, vol. 75, pp. 234–247, 2018.

[11] R. S. Merifield, A. V. Lyamin, and S. W. Sloan, "Three-dimensional lower-bound solutions for the stability of plate anchors in sand," *Geotechnique*, vol. 56, no. 2, pp. 123–132, 2006.

[12] H. Mokhbi, M. Mrllas, A. Mabrouki, and J.-M. Pereira, "Three-dimensional numerical and analytical study of horizontal group of square anchor plates in sand," *Acta Geotechnica*, vol. 13, no. 1, pp. 159–174, 2018.

[13] J. P. Sahoo and J. Kumar, "Vertical uplift resistance of two interfering horizontal anchors in clay," *Journal of Geotechnical and Geoenviromental Engineering*, vol. 140, no. 4, 2014.

[14] Y. J. Al Shakarchi, M. Y. Fattah, and I. K. Kashat, "The behaviour of batter piles under uplift loads," in *International Conference on Geotechnical Engineering, University of Sharjah, October 3-6, 2004*, pp. 105–114, Sharjah, UAE, 2004.

[15] S. H. Chow, C. D. O'Loughlin, C. Gaudin, and J. T. Lieng, "Drained monotonic and cyclic capacity of a dynamically installed plate anchor in sand," *Ocean Engineering*, vol. 148, pp. 588–601, 2018.

[16] J. R. Giampa, A. S. Bradshaw, and J. A. Schneider, "Influence of dilation angle on drained shallow cicular anchor uplift capacity," *International Journal of Geomechanics*, vol. 17, no. 2, 2017.

[17] B. M. Das, S. K. Shukla, Earth Anchors et al., "Numerical investigation of group anchors," in *the Internatonal Foundations Congress and Equipmenr Espo, San Antonio, TX*, pp. 279–288, American Society of Civil Engineers, Renton, VA, 2015.

[18] H. Niroumand and K. A. Kassim, *Design and Cinstruction of Soil Anchor Plates*, Butterworth-Heinemann, Oxford, United Kingdom, 2016.

[19] Y. J. Al-Shakarchi, M. Y. Fattah, R. H. Abood, W. H. Shgeet, and K. Abdlhussein, "Experimental and theoretical study by the finite element on horizontal anchors in sandy soil," *The Journal of the Arab Universities Associations and the Engineering Researches*, vol. 9, no. 2, pp. 135–155, 2003.

[20] F. M. Abdrabbo and A. Z. El Wakil, "Laterally loaded helical piles in sand," *Alexandria Engineering Journal*, vol. 55, no. 4, pp. 3239–3245, 2016.

[21] S. Mittal, B. Ganjoo, and S. Shekhar, "Static equilibrium of screw anchor pile under lateral load in sands," *Geotechnical and Geological Engineering*, vol. 28, no. 5, pp. 717–725, 2010.

[22] N. Zhu, L. Cui, J. Liu, M. Wang, H. Zhao, and N. Jia, "Discrete element simulation on the behavior of open-ended pipe pile under cyclic lateral loading," *Soil Dynamics and Earthquake Engineering*, vol. 144, article 106646, 2021.

[23] C. Y. Wang, H. L. Liu, X. M. Ding, and C. L. Wang, "Study on the horizontal bearing characteristics of pile foundation in coral sand," *Canadian Geotechnical Journal*, vol. 99, no. 999, pp. 1928–1942, 2021.

[24] Y. F. Fan, J. H. Wang, and S. L. Feng, "Effect of spudcan penetration on laterally loaded pile groups," *Ocean Engineering*, vol. 221, article 108505, 2021.

[25] B. X. Yuan, M. Sun, L. Xiong, Q. Z. Luo, S. P. Pradhan, and H. Z. Li, "Investigation of 3D deformation of transparent soil around a laterally loaded pile based on a hydraulic gradient model test," *Journal of Building Engineering*, vol. 28, no. 3, article 101024, 2020.

[26] B. X. Yuan, K. Xu, Y. X. Wang, R. Chen, and Q. Z. Luo, "Investigation of deflection of a laterally loaded pile and soil deformation using the PIV technique," *International Journal of Geomechanics*, vol. 17, no. 6, article 04016138, 2017.

[27] X. L. Zhang, X. J. Yuan, X. C. Shun, and L. K. Yuan, "An analysis method for lateral capacity of pile foundation under existing vertical loads," *Soil Dynamics and Earthquake Engineering*, vol. 142, 2021.

[28] C. Y. C. Cheuk, D. J. White, and M. D. Bolton, "Uplift mechanisms of pipes buried in sand," *Journal of Geotechnical and Geoenvironmental Engineering*, vol. 134, no. 2, pp. 154–163, 2008.

[29] C. Liu, W. T. Tang, H. W. Wei, P. P. Wang, and H. H. Zhao, "Model tests of jacked-pile penetration into sand using transparent soil and incremental particle image velocimetry," *Geotechnical Engineering*, vol. 24, no. 4, pp. 1128–1145, 2020.

[30] T. Jiang, L. J. Wang, J. R. Zhang, and H. Jia, "Effect of water content on near-pile silt deformation during pile driving using PIV technology," *Geomechanics and Engineering*, vol. 23, no. 2, pp. 139–149, 2020.

[31] D. J. White, W. A. Take, and M. D. Bolton, "Soil deformation measurement using particle image velocimetry (PIV) and photogrammetry," *Géotechnique*, vol. 53, no. 7, pp. 619–631, 2003.

[32] Y. L. Yang, M. L. Qi, J. Z. Li, and D. D. Ma, "Experimental study of flow field around pile groups using PIV," *Experimental Thermal and Fluid Science*, vol. 120, article 110223, 2021.

[33] B. X. Yuan, J. Y. Liu, W. W. Chen, and K. W. Xia, "Development of a robust stereo-PIV system for 3-D soil deformation measurement," *Journal of Testing and Evaluation*, vol. 40, no. 2, article 103856, 2012.

[34] Z. J. You and Y. L. Chen, "The use of tactile sensors and PIV analysis for understanding the bearing mechanism of pile groups," *Sensors*, vol. 18, no. 2, p. 476, 2018.

[35] J. Y. Liu, M. Liu, and Z. Zhu, "Sand deformation around an uplift plate anchor," *Journal of Geotechnical and Geoenvironmental Engineering*, vol. 138, no. 6, pp. 728–737, 2012.

[36] X. Zhang, J. Y. Liu, and M. L. Liu, "Experimental study on uplift behavior of group anchors in sand," *Geotechnical Testing Journal*, vol. 42, no. 3, pp. 687–702, 2019.

[37] Ministry of Water Resources of the People's Republic of China, *GB/T 50123-2019 Standard for Geotechnical Testing Method*, Ministry of Housing and Urban-Rural Development of the People's Republic of China, Beijing, 2019.